S-Nitrosation of cysteine as evidenced by IRMPD spectroscopy

ARTICLE *in* INTERNATIONAL JOURNAL OF MASS SPECTROMETRY · JULY 2012

Impact Factor: 1.97 · DOI: 10.1016/j.ijms.2012.07.003

International Journal of Mass Spectrometry xxx (2012) xxx–xxx

Contents lists available at SciVerse ScienceDirect

International Journal of Mass Spectrometry

journal homepage: www.elsevier.com/locate/ijms

S-nitrosation of cysteine as evidenced by IRMPD spectroscopy

Francesco Lanucara[a,1], Barbara Chiavarino[a], Maria Elisa Crestoni[a], Debora Scuderi[b], Rajeev K. Sinha[a,2], Philippe Maître[b], Simonetta Fornarini[a,*]

[a] Dipartimento di Chimica e Tecnologie del Farmaco, Università di Roma "La Sapienza", P.le A. Moro 5, 00185 Roma, Italy
[b] Université Paris Sud, Laboratoire de Chimie Physique, UMR8000 CNRS Faculté des Sciences, Bâtiment 350, 91405 Orsay Cedex, France

ARTICLE INFO

Article history:
Received 11 May 2012
Received in revised form 25 June 2012
Accepted 4 July 2012
Available online xxx

Dedicated to professor Peter B. Armentrout on the occasion of his 60th birthday.

Keywords:
Nitrosothiol
Nitrosation
Structure elucidation
IR spectroscopy
Gaseous ions
Density functional calculations

ABSTRACT

S-nitrosation of cysteine plays an important role in storage and transport of NO, a key signaling molecule in vivo. An approach to detect this modification in the bare, charged amino acid is presented, based on IR multiple photon dissociation (IRMPD) spectroscopy. Protonated and deprotonated S-nitrosocysteine ions, $[SNOCys+H]^+$ and $[SNOCys-H]^-$, have been obtained by electrospray ionization and assayed for IR activity in either the 1000–1900 cm^{-1} or the 3000–3600 cm^{-1} wavenumber range. The so-obtained IRMPD spectra display characteristic features ascribed to the presence of the S-nitrosation motif, which are missing in the corresponding IRMPD spectra of the native cysteine ions, $[Cys+H]^+$ and $[Cys-H]^-$. In particular, the NO stretching mode is unambiguously identified by the red shift observed for the ^{15}N-labelled species. The interpretation of the IRMPD spectra is supported by density functional theory calculations of the optimized geometries, relative energies and IR spectra of $[SNOCys+H]^+$ and $[SNOCys-H]^-$. Both sampled ions comprise a thermally averaged population of conformers contributing to the experimental IRMPD spectra. This notion is supported by the agreement between the convoluted IR spectra of the several conformers, and the recorded IRMPD spectrum. The gathered evidence points to a characteristic NO stretching mode that emerges as a pronounced feature at 1460–1490 cm^{-1} in the IRMPD spectrum of $[SNOCys-H]^-$, namely in a region where $[Cys-H]^-$ displays no IRMPD activity. Conversely, the NO stretching vibration of $[SNOCys+H]^+$ is enclosed in a wide absorption including the C=O stretching mode at 1780 cm^{-1}. The $[SNOCys-H]^-$ negative ions are thus a promising benchmark in a search for S-nitrosation features using IRMPD spectroscopy.

1. Introduction

S-nitrosation or thionitrite formation (also commonly referred to as S-nitrosylation) has emerged as one of the most important mechanisms of NO signaling. Accumulating evidence suggests that S-nitrosothiols play key roles in human health and disease which accounts for the great interest in their chemistry as reported in the past decade [1–5]. S-nitrosocysteine (SNOCys) is the prototypical compound for the S-nitrosothiols naturally occurring in vivo that are responsible for the endogenous storage and transport of NO. Directly related to the ability to donate NO, SNOCys is also one of the more unstable biologically relevant S-nitrosothiols and characterizing this species is not a trivial task [6–9]. In the present contribution infra-red multiple photon dissociation (IRMPD) spectroscopy, based on the use of an IR radiation source of high power and wide tunability combined with tandem mass spectrometry, has been exploited to gain insight into the structural and spectroscopic features of ions derived from SNOCys. The ions delivered into the gas phase by electrospray ionization are either the protonated molecule, $[SNOCys+H]^+$, or the deprotonated species $[SNOCysNO-H]^-$. The high degree of in-depth information that can be gained by IRMPD spectroscopy of the ionic species obtained from the natural amino acids is well illustrated in several recent papers and review articles [10–27]. In particular, a notable effort has been devoted to ascertain the conditions favoring zwitterionic structures and to unambiguously characterize them. The sample ions obtained by protonation or deprotonation of native cysteine ($[Cys+H]^+$ and $[Cys-H]^-$, respectively) have been already assayed by IRMPD spectroscopy in the 600–1800 cm^{-1} IR range and the experimental spectra have been discussed in association with the calculated IR spectra of the most stable conformers in two landmark papers [28,29]. The deprotonated cysteine ion has been probed as model ion in view of the current interest about the structure of ions formed by electrospray ionization (ESI) [30–33]. Whether they

* Corresponding author. Fax: +39 06 4991 3602.
E-mail address: Simonetta.fornarini@uniroma1.it (S. Fornarini).
[1] Prtesent address: School of Chemistry, University of Manchester, Manchester Interdisciplinary Biocentre, 131 Princess Street, Manchester M1 7ND, UK.
[2] Prtesent address: Centre for Atomic and Molecular Physics, Manipal University, Karnataka 576104, India.

1387-3806/$ – see front matter © 2012 Elsevier B.V. All rights reserved.
http://dx.doi.org/10.1016/j.ijms.2012.07.003

retain their former structure in solution or rather adopt the one thermodynamically favored in the gas phase is a topic of active investigation and debate. The deprotonated cysteine ion displays an experimental IRMPD spectrum consistent with a carboxylate structure (deprotonation on the COOH group) although the thiolate structure (deprotonation on the SH group) is calculated to be lower in energy [30,34,35].

$[Cys+H]^+$ and $[Cys-H]^-$ ions are now re-examined as reference species to aid in identifying distinctive signatures for the nitrosation feature in the IRMPD spectra of $[SNOCys+H]^+$ and $[SNO-Cys-H]^-$.

2. Experimental details

2.1. Materials

L-Cysteine hydrochloride, $NaNO_2$, $Na^{15}NO_2$ and all the solvents used in this work were research grade products from commercial sources (Sigma–Aldrich s.r.l. Milan, Italy) and were used without any further purification. S-nitrosocysteine was obtained from the reaction of L-cysteine (2 mM) and $NaNO_2$ or $Na^{15}NO_2$ (2 mM) in H_2O:CH_3CN 1:1 (2 ml) at 37 °C, by adding H_2SO_4 (98%) to the reaction mixture to pH 1.5, followed by a 1 in 100 dilution in H_2O:CH_3CN 1:1. An alternative method has also been assayed, allowing L-cysteine (20 mM in H_2O:CH_3CN) to react with NO (1 bar) after purging the solution and the flask repeatedly with Ar. UV–vis spectroscopy has been used to confirm the formation and stability of S-nitrosocysteine by monitoring the presence of the band at 543 nm assigned to an $n \rightarrow \pi^*$ charge-transfer transition. Soon after preparation of the compound (which occurs on mixing), diluted solutions (about 7 μM) for ESI-MS experiments were prepared. ESI-MS analysis shows the protonated molecule $[SNOCys+H]^+$ at m/z 151, the protonated disulfide (protonated cystine) at m/z 241 and the cysteine radical cation at m/z 121. The deprotonated amino acids are generated by ESI of 0.1 mM solutions in H_2O:CH_3CN 1:1 by the addition of NH_3 to assist deprotonation.

2.2. IRMPD experiments

IRMPD experiments on the protonated and deprotonated forms of S-nitrosocysteine and cysteine have been performed in two spectral regions, namely 1000–2000 cm^{-1} and 3200–3600 cm^{-1}, using two different IR radiation sources, the free electron laser (FEL) at the Centre Laser Infrarouge d'Orsay (CLIO) facility and an Optical Parametric Oscillator/Amplifier (OPO/OPA) laser system at the Università di Roma "La Sapienza", respectively. The FEL radiation is generated by a 10–50 MeV electron linear accelerator and is delivered in 8 μs-long macropulses at a repetition rate of 25 Hz, each containing 500 micropulses (1–2 ps long). Typical macropulse energies are 40 mJ. Ions were irradiated with 4–10 macropulses. For the present study, the FEL was operated at 45 MeV in order to optimize the laser power in the frequency region of interest. The laser wavelength profile was monitored at each reading with a monochromator associated with a pyroelectric detector array (spiricon).

The FEL based experiment was performed using a hybrid FT-ICR tandem mass spectrometer (APEX-Qe Bruker) equipped with a 7.0 T actively shielded superconducting magnet and a quadrupole–hexapole interface for mass-filtering and ion accumulation, under control by the commercial software APEX 1.0. Protonated and deprotonated cysteine and S-nitrosocysteine ions were mass-selected in the quadrupole and accumulated in a hexapole containing argon buffer gas for 0.5 s prior to their transfer into the ICR cell where they were exposed to the IR FEL radiation.

An OPO/OPA laser source (LaserVision) coupled to a Paul ion trap tandem mass spectrometer (Esquire 6000+, Bruker Inc.) is employed to explore the 3200–3600 cm^{-1} spectral region of protonated cysteine and S-nitrosocysteine. This parametric converter is pumped by a non-seeded Nd:YAG laser (Continuum Surlite II) operating at 10 Hz repetition rate. The typical pulse width of this pump laser is 4–6 ns with output pulse energy of 600 mJ at 1064 nm. In the trap, ions were accumulated for 50 ms and mass selected prior to IR irradiation. The typical irradiation time used in the experiment is 1 s. The irradiation time is controlled using an electromechanical shutter synchronized precisely with the mass spectrometer.

The IRMPD spectrum is obtained by plotting the photofragmentation yield R ($R = -\ln[I_{parent}/(I_{parent} + \Sigma I_{fragments})]$, where I_{parent} and $I_{fragments}$ are the integrated intensities of the mass peaks of the precursor and of the fragment ions, respectively) as a function of the frequency of the IR radiation [36,37].

2.3. Computational details

The reported computational data are obtained using the hybrid density functional method B3LYP in conjunction with the 6-311++G** basis sets. This platform (or a slightly lower level of theory such as B3LYP/6-31++G** [29] or B3LYP/6-311G** [28]) has been found to perform well for protonated and deprotonated amino acids. For the deprotonated species calculations have been run also at B3LYP/cc-pVTZ level, however no sizeable differences were observed. For all optimized structures, frequency analyses at the same level of theory were performed in order to assign these structures as genuine minima as well as to calculate harmonic vibration frequencies and zero-point vibrational energies. A conformational survey was made in order to select the most stable conformers for cysteine and S-nitrosocysteine in their protonated and deprotonated forms [38]. All calculations were performed using the Gaussian 03 or Spartan 08 software packages. The procedure first involved a conformational search, using the MMFF molecular mechanics model. Out of 10,000 conformers examined, the lowest energy 30–50 structures were kept for each species and used as starting geometries for hybrid DFT calculations at increasing levels of theory. While there is no absolute certainty that the global minimum will actually be identified, we note that the most stable conformers of the protonated and deprotonated forms of cysteine or S-nitrosocysteine generally agree with the most stable geometries previously reported [28,29,39]. Ultimately, geometries and harmonic vibrational frequencies were obtained at B3LYP/6-311++G** level. The relative energies at 0 K were converted to relative free energies at 298 K using the rigid rotor/harmonic oscillator approximation and using unscaled harmonic frequencies.

In order to obtain IR spectra for the species of interest to be compared with the experimental IRMPD spectra, the calculated harmonic vibrational frequencies were scaled by a factor of 0.985 in the 1000–2000 cm^{-1} region and 0.955 in the 3000–3700 cm^{-1} frequency range [40]. For the NO stretch the mode specific factor of 0.940 was adopted [41–43]. In the figures comparing the experimental IRMPD spectra with the computed spectra, the calculated absorption lines are convoluted with a Lorentzian profile of 20 cm^{-1} fwhm (full width at half maximum) in the 1000–2000 cm^{-1} region while a fwhm of 10 cm^{-1} was used for the 3000–3700 cm^{-1} frequency range. Because several conformers very close in energy are present in the sampled ion population a thermally averaged spectrum has been composed, where the IR intensities for the individual conformers are scaled by a factor f_i assuming a Maxwell–Boltzmann distribution at 298 K.

$$f_i = \frac{e^{-(\Delta G^\circ/RT)i}}{\sum_j e^{-(\Delta G^\circ/RT)i}}$$

Please cite this article in press as: F. Lanucara, et al., Int. J. Mass Spectrom. (2012), http://dx.doi.org/10.1016/j.ijms.2012.07.003

3. Results and discussion

3.1. Photodissociation of S-nitrosocysteine ions

Electrospray ionization of a dilute, freshly prepared solution of S-nitrosocysteine (SNOCys) affords the gaseous protonated species $[SNOCys+H]^+$ (ions at m/z 151) which has been selected and studied. The fragmentation of $[SNOCys+H]^+$ upon irradiation by IR photons in resonance with an active vibrational mode proceeds by the exclusive loss of NO, yielding ions at m/z 121 (Fig. 1Sa in the supplementary data). A mass shift of one unit for the protonated molecule (m/z 152) is observed when $Na^{15}NO_2$ is used as the nitrosation agent. Photofragmentation of the ion at m/z 152 results in ^{15}NO loss giving the same fragment ion at m/z 121 (Fig. 1Sb).

The same loss of neutral NO is observed when $[SNOCys+H]^+$ ions undergo fragmentation under collision induced dissociation (CID) conditions. A detailed study of the CID process has been reported and the reaction pathway and associated structures have been probed by DFT calculations [39]. Regarding the structure of the ESI-formed $[SNOCys+H]^+$ ion, both DFT calculations at B3LYP/6-311++G** level and experimental evidence point to a species protonated on the amino group [39,40]. Imparting excess internal energy onto this species, the facile homolytic S—N bond cleavage leads to a distonic cysteine radical cation holding a protonated amino group and a radical site on the sulfur atom [Eq. (1)]. This structure has been probed by IRMPD spectroscopy [40] and a homologous one has been identified for the ionic product of NO loss from protonated S-nitrosocysteine methyl ester [44].

$$H_3N^+CH(CH_2SNO)CO_2H \rightarrow H_3N^+CH(CH_2S^\bullet)CO_2H + NO^\bullet \quad (1)$$

When the NO loss is compared with competing paths, (U)B3LYP/6-311++G** calculations have shown that this dissociation route is occurring due to kinetic reasons [39]. The activation energy is in fact lower than the one pertaining to the formation of the thermodynamically favored products involving H_2O and CO losses. The size of the activation energy for NO cleavage, which has been evaluated to exceed the endothermicity of the process by 24 kJ mol^{-1} [39], requires the absorption of multiple (more than ten) photons in the mid-IR range in order to reach the fragmentation threshold and to observe efficient photofragmentation.

For comparison purposes IRMPD spectroscopy has been performed also on the protonated cysteine ion $[Cys+H]^+$. This species has already been examined in the 600–1800 cm^{-1} range [28] while the IRMPD spectrum in the NH/OH stretching region is reported here for the first time. In both regions, the most abundant photofragment ion at m/z 76 involves $CO+H_2O$ loss. Minor fragments at m/z 105 and 87 are ascribed to losses of NH_3 and NH_3+H_2O, respectively [45]. An exemplary mass spectrum obtained when $[Cys+H]^+$ ions are irradiated at 3545 cm^{-1} is shown in Fig. 2S.

The photofragmentation of $[SNOCys-H]^-$ yields ions at m/z 59, 62, 73, and 88 (Fig. 3Sa in the supplementary data). The major product ion at m/z 62 (SNO^-) finds a counterpart in the fragmentation of the reference $[Cys-H]^-$ ion leading to a product ion at m/z 33 (HS^-), as already reported both under IRMPD and CID conditions [29,46]. This ion shifts in fact at m/z 63 when the parent ion is labelled with ^{15}N on the nitroso group (Fig. 3Sb).

3.2. IRMPD spectroscopy of protonated S-nitrosocysteine (^{15}N-labelling and comparison with $[Cys+H]^+$ ions)

The IRMPD spectrum of $[SNOCys+H]^+$ in the 900–1900 wavenumber range is plotted in Fig. 1a (black profile). It shows three relatively wide features centered at 1167, 1443, and 1783 cm^{-1}. These features may be compared with the three bands at 1161, 1436, and 1761 cm^{-1} which characterize the IRMPD spectrum of $[Cys+H]^+$, shown in Fig. 1b. The latter spectrum has already been described and band positions have been recorded at about 1150, 1430, and 1774 cm^{-1} [28]. The fair correspondence of the two spectra allows one to tentatively assign the vibrational modes responsible for the observed features in the IRMPD spectrum of $[SNOCys+H]^+$ as already depicted for the IRMPD spectrum of $[Cys+H]^+$, namely the C=O stretching at 1783 and 1761 cm^{-1}, the NH_3 umbrella mode at 1443 and 1436 cm^{-1} and skeletal flex and COH bending motions at 1167 and 1161 cm^{-1}, for the S-nitroso and the native species, respectively.

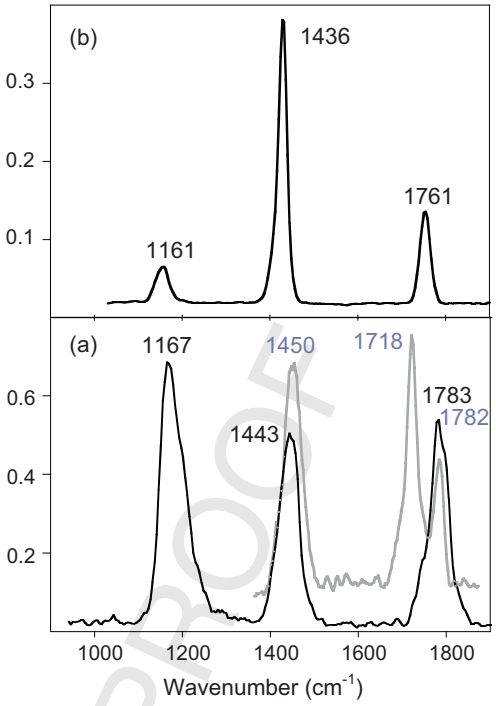

Fig. 1. IRMPD spectrum of $[SNOCys+H]^+$ (a) and of $[Cys+H]^+$ (b) in the 900–1900 cm^{-1} wavenumber range. The grey profile in panel (a) reports the (partial) IRMPD spectrum of $[S^{15}NOCys+H]^+$.

The similarity of the two spectra could have been anticipated on the basis of the comparable molecular structure, differing only for the presence of a SNO in the place of a SH group. However, any characteristic S-nitrosation signatures in the IR region explored seemingly fails to appear for this protonated species. The NO stretching mode is expected near 1716 cm^{-1}, as found for protonated S-nitrosocaptopril, a biologically active S-nitrosothiol [47]. It appears that in the case of $[SNOCys+H]^+$ this mode is either poorly active or enclosed with another absorption. In order to gain insight into this point, the ^{15}NO-labelled ion $[S^{15}NOCys+H]^+$, has been prepared and analyzed, anticipating a sizeable red shift for the ^{15}NO stretching vibration with respect to the unlabelled species. The IRMPD spectrum is reported in Fig. 1a as the grey profile. In this spectrum, while the mode at 1443 cm^{-1} absorbs at about the same wavenumber (1450 cm^{-1}), the band at 1783 cm^{-1} is now replaced by two partly overlapping bands with maxima at 1718 and 1782 cm^{-1}. Because the NO oscillator is expected to show a red-shift upon ^{15}N-labelling, the spectrum of this isotopologue species allows us to assign the C=O stretching at 1782 and the ^{15}NO stretching at 1718 cm^{-1}. The NO stretching mode is clearly not resolved in the unlabelled species, merging into one band with the C=O stretching vibration.

$[SNOCys+H]^+$ and $[Cys+H]^+$ ions have been examined also in the NH/OH stretching region and the two IRMPD spectra are shown in Fig. 2, panel a and b, respectively. The two ions share very similar absorptions also in this spectral range. The major feature at

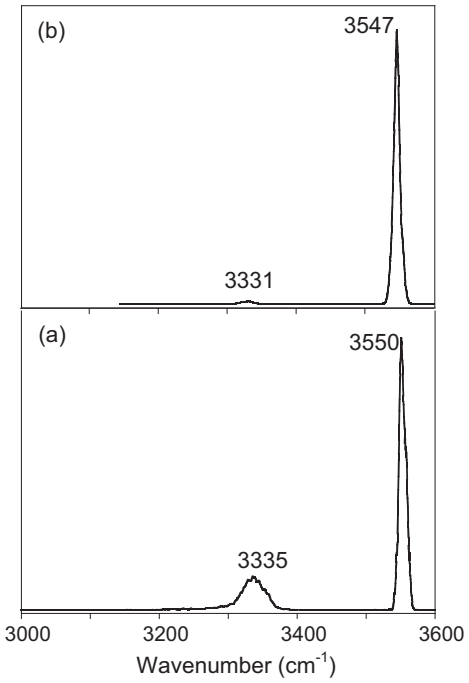

Fig. 2. IRMPD spectrum of $[SNOCys+H]^+$ (a) and of $[Cys+H]^+$ (b) in the 3000–3600 cm^{-1} wavenumber range.

3550 cm^{-1} for $[SNOCys+H]^+$ and at 3547 cm^{-1} for $[Cys+H]^+$ ions is ascribed to the OH stretching vibration of the carboxyl group. The second feature at 3335 and 3331 cm^{-1} for $[SNOCys+H]^+$ and $[Cys+H]^+$ ions, respectively, can be assigned to the stretching vibration of the NH bond not involved in hydrogen bonding, as observed for other gaseous protonated aminoacids such as tyrosine and phenylalanine [48], nitrotyrosine [38], and phosphotyrosine [49].

3.3. Interpretation of IRMPD spectra of $[SNOCys+H]^+$ ions and calculated IR spectra

Insights into the features pertaining to the experimental IRMPD spectra can be gained from the computed IR spectra of the species that reasonably account for the sampled ion population. To this end, a survey of the most stable conformers has been performed. Stable conformers of $[SNOCys+H]^+$ ions, **1a**–**g**, bearing the additional proton on the amino group are depicted in Fig. 3. The relative free energies at 298 K are given in parentheses in kJ mol^{-1} and thermodynamic data are listed in Table 1S. The most stable conformer **1a** shows interatomic distances indicating that two of the three hydrogen atoms of the $-NH_3^+$ group are engaged in H-bonding with the carbonyl oxygen and the sulfur atom, respectively. Similar features characterize also species **1b**–**f** so it is not surprising that the IR spectra of **1a**–**f** are very similar to each other both in the mid-IR and in the O–H/N–H stretching region. Conformer **1g**, relatively higher in free energy, is characterized by the N atom (rather than S) of the SNO group here engaged in H-bonding. The SNO group may adopt either a syn or an anti configuration, which appears, respectively, in the isomeric couples **1c**/**1e** and **1d**/**1f**. However, the syn/anti configuration appears to have only minor effects both on the relative free energy and on the IR spectrum. Thus, the IRMPD spectrum cannot be expected to hold any diagnostic hint about this structural motif.

Table 1
Spectral position of IRMPD bands of protonated S-nitrosocysteine ($[SNOCys+H]^+$) ions observed in the molecular fingerprint region as well as in the O–H/N–H stretching region.

Experimental IRMPD[a]	Vibrational mode
1167	Skeletal flex and COH bend
1443	NH_3 umbrella
1783	C=O stretch, NO stretch
3331	NH stretch (free)
3547	OH stretch
1450[b]	NH_3 umbrella
1718[b]	^{15}NO stretch
1782[b]	C=O stretch

[a] In cm^{-1}.
[b] Experimental IRMPD frequencies of ^{15}N-labelled $[Cys^{15}NO+H]^+$.

The calculated IR spectra of **1a**–**g** in the two IR ranges are plotted in Figs. 4S and 5S, respectively. The calculated IR harmonic frequencies obtained by hybrid DFT calculations have been scaled by appropriate factors to match the experimental IR features [50–52]. In particular, the NO stretching vibration is known to be an exceptional case [41–43] because the hybrid DFT calculated frequency tends to be rather higher than the experimental one and for this mode a factor of 0.940 has been used. A direct comparison of the experimental IRMPD spectrum with the calculated IR spectra of the most stable conformers further requires an appropriate weighing of the conformer relative abundances, which is obtained by considering the Maxwell–Boltzmann distribution at 298 K. The experimental spectrum is plotted together with the weighted average of the IR spectra of **1a**–**g** in Fig. 4a The remarkably good agreement suggests that the sampled ion population is appropriately analyzed. This notion is further supported by the fair correspondence of the plots in Fig. 4b showing the IRMPD spectrum of the ^{15}NO-labelled ion and the profile of the convoluted IR spectra for the Maxwell–Boltzmann averaged population of conformers.

The calculated IR spectra and animation of the individual resonances allow a final assignment to the experimental IRMPD bands, consistent with the assignments illustrated in the previous paragraph. The relevant data are listed in Table 1.

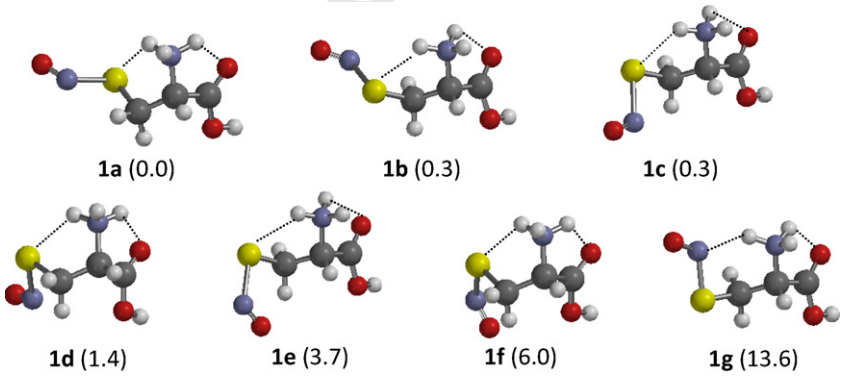

Fig. 3. Most stable conformers of $[SNOCys+H]^+$ and relative free energies at 298 K (kJ mol^{-1}) calculated at B3LYP/6-311++G** level of theory.

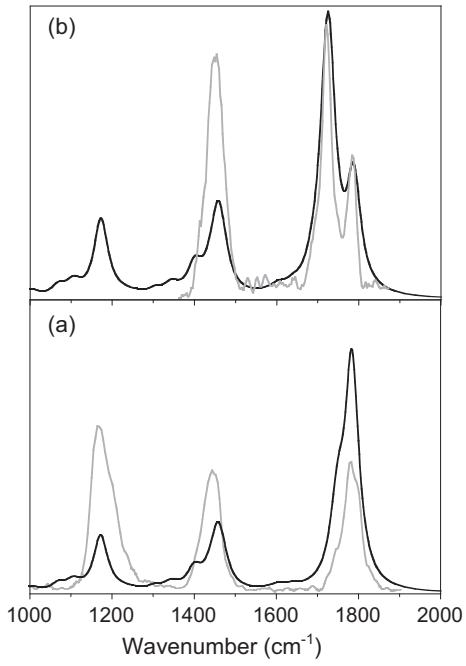

Fig. 4. IRMPD spectra of $[SNOCys+H]^+$ (a) and of $[S15NOCys+H]^+$ (b) (in grey). In each panel the black line is a convolution of calculated IR frequencies with intensities weighted according to the Maxwell–Boltzmann distribution of conformers in the sampled ion population.

3.4. IRMPD spectroscopy of $[SNOCys-H]^-$ ions (^{15}N-labelling and comparison with $[Cys-H]^-$ ions)

The IRMPD spectrum of $[SNOCys-H]^-$ ions in the IR fingerprint region is shown in Fig. 5a. As observed in the IRMPD spectrum of the positive $[SNOCys+H]^+$ ions, three strong features are present, namely a band at 1324 cm^{-1} and two wide absorptions with maxima at 1460–1488 and 1660 cm^{-1}. However, a remarkable difference with the positive ions appears in comparing the IRMPD spectrum of $[SNOCys-H]^-$ with the one of the native aminoacid $[Cys-H]^-$. As shown in Fig. 5b and already described [29], deprotonated cysteine displays only two IRMPD features in the 1200–1800 cm^{-1} range, at 1324 and 1634 cm^{-1}. Reported absorptions are at 1315 and 1630 cm^{-1} with no significant activity in between [29]. The strongest band at higher frequency has been ascribed to the asymmetric C–O stretch of a carboxylate structure for deprotonated cysteine while the band at 1315 (1324 cm^{-1} in this paper) is assigned to the symmetric stretch of the $-CO_2^-$ group. Because this group is present as well in $[SNOCys-H]^-$, the bands at 1324 and at 1660 cm^{-1} share the same origin as in the native aminoacid anion. The S-nitrosation event is then responsible for the appearance of the feature at 1460–1488 cm^{-1}. This point is further clarified by recording the IRMPD spectrum of the ^{15}N-labelled ion $[S^{15}NOCys-H]^-$. The spectrum of this species, plotted in Fig. 5a as the grey profile, shows a nearly exact matching relative to the one of the unlabelled ion with the notable exception of the wide feature at 1460–1488 cm^{-1}, which is now shifted at 1418–1454 cm^{-1}.

A distinct redshift of about this size is indeed expected for an NO oscillator upon ^{14}N to ^{15}N substitution as already observed in IRMPD spectra of ionic species bearing a nitroso group [42,53,54]. This result supports an assignment to the NO stretching vibration of the characteristic SNO group.

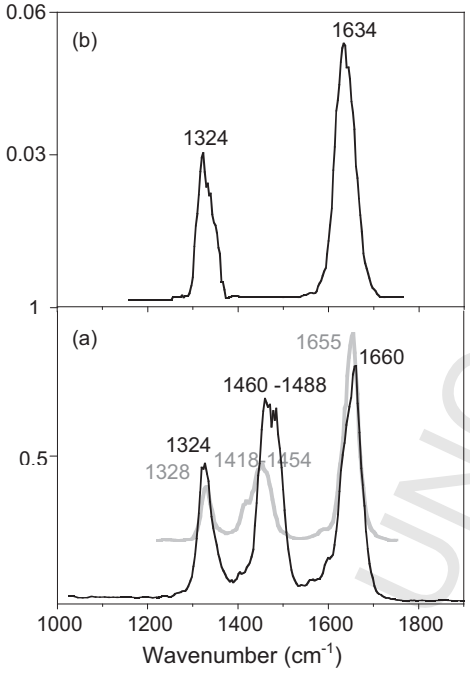

Fig. 5. IRMPD spectrum of $[SNOCys-H]^-$ (a) and of $[Cys-H]^-$ (b) in the 1000–1900 cm^{-1} wavenumber range. The grey profile in panel (a) reports the (partial) IRMPD spectrum of [S15NOCys–H]–.

3.5. Interpretation of IRMPD spectra of $[SNOCys-H]^-$ ions and calculated IR spectra

As already described for the protonated species, also $[SNOCys-H]^-$ ions present a large array of conformers. The optimized structures of the most stable ones, **2a**–**l**, are displayed in Fig. 6 and the calculated IR spectra in the 1000–2000 cm^{-1} wavenumber range are illustrated in Fig. 6S. The relative free energies at 298 K are given in parentheses in kJ mol^{-1} (Fig. 6) and thermodynamic data are listed in Table 2S. A structural element that is common to all species, **2a**–**l**, is a hydrogen bond linking the amino and carboxylate groups. The asymmetric C–O stretch of $-CO_2^-$ is associated with a pronounced band at 1635–1665 cm^{-1}, at a relatively constant frequency for the various conformers. A second highly active vibration in the IR spectra is associated with the NO stretching mode, whose frequency is affected by a larger variation, spreading between 1430 and 1495 cm^{-1}.

The SNO group may adopt either a syn or an anti configuration, which appears, respectively, in species **2a**, **d**, **e**, **h**, **j**, **k** and **2b**, **c**, **f**, **g**, **i**, **l**. *S*-Nitrosothiols exhibit properties suggesting considerable S—N double bond character and an appreciable barrier to rotation [55–58]. Hindered rotation about the S—N bond exists also within $[SNOCys-H]^-$ ions. For example, the barrier separating **2d** from **2b** amounts to 58 kJ mol^{-1} (see the energy profile reported in Fig. 7S), in good agreement with a barrier of similar size, 46 kJ mol^{-1}, determined experimentally for the interconversion of S-nitroso alkylthiols [56,57]. However, the syn/anti geometry has only a minor effect on the energy of the two isomers (Table 2S) [55,56] and also on the relative free energies reported in Fig. 6 where the data for the syn isomers **2a**, **d**, **e**, **h**, **j**, **k** differ by less than 1 kJ mol^{-1} from the values of each corresponding anti isomer, namely in the order **2c**, **b**, **f**, **l**, **i**, **g**.

The syn versus anti configuration of the SNO group appears also to have hardly any influence on the IR spectra of the conformers reported in Fig. 6S, at most displacing the NO stretch by few cm^{-1} to the blue going from the syn to the anti form. However, the remarkable feature in the IR spectra of **2a**–**l** is indeed the NO stretching mode. It yields a highly intense IRMPD band in a spectral region where $[Cys-H]^-$ shows no appreciable activity (Fig. 5) [29]. Animation of the vibrational modes confirms the assignment of the experimental IRMPD bands drawn from the comparison with

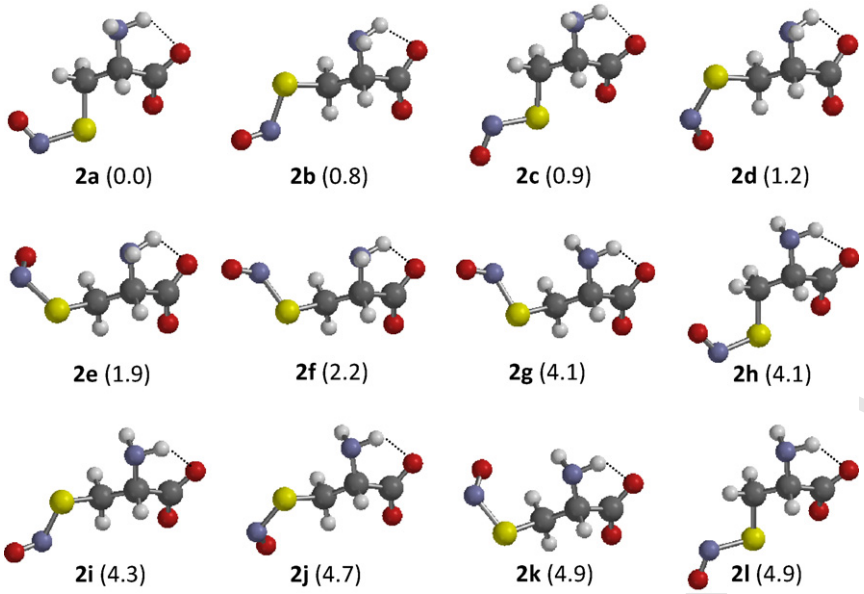

Fig. 6. Most stable conformers of $[SNOCys-H]^-$ and relative free energies at 298 K (in parentheses, kJ mol^{-1}) calculated at B3LYP/6-311++G** level of theory.

the spectrum of $[Cys-H]^-$ ions, as described in Table 2. However, for a more quantitative appraisal, the IRMPD spectrum has been evaluated against the calculated IR spectra of the most stable conformers displayed in Fig. 6S. In order to account for the presence of several conformers contributing to the sampled $[SNOCys-H]^-$ ions, in the unlabelled as well as in the ^{15}N-labelled species, the individual IR modes of the conformers have been weighted according to the Maxwell–Boltzmann distribution at the estimated temperature of the experiment (298 K). The fine matching of the experimental IRMPD spectrum and the convolution of the calculated IR spectra is illustrated in Fig. 7a. The IRMPD spectrum of the ^{15}N-labelled species is reported in Fig. 7b together with the same Maxwell–Boltzmann weighted convolution of IR spectra, the only difference being the presence of the ^{15}NO oscillator replacing ^{14}NO. The agreement is consistently good, confirming both the characteristics of the sampled ion population and the satisfactory interpretation of the experimental data.

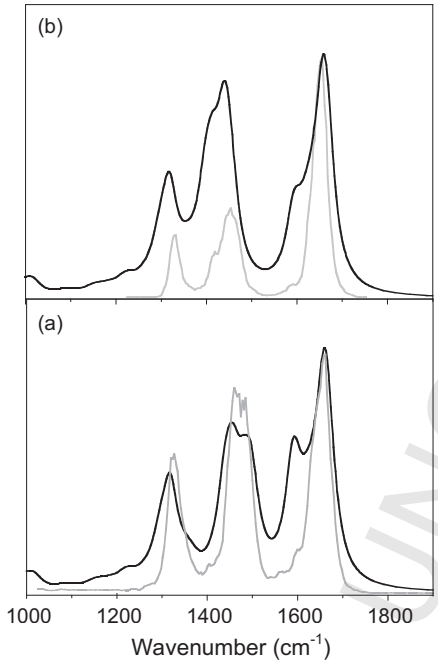

Fig. 7. IRMPD spectrum of $[SNOCys-H]^-$ (a) and of $[S^{15}NOCys-H]^-$ (in grey) (b). In each panel the black line is a convolution of calculated IR frequencies with intensities weighted according to the Maxwell–Boltzmann distribution of conformers in the sampled ion population.

Table 2
Spectral position of IRMPD bands of deprotonated S-nitrosocysteine ($[SNOCys-H]^-$) ions in the molecular fingerprint region.

Experimental IRMPD[a]	Vibrational mode
1324	Symm C–O stretch and skeletal flex
1460–1488	NO stretch
1660	Asymm C–O stretch (+NH_2 scissor)
1328[b]	Symm C–O stretch and skeletal flex
1418–1454[b]	^{15}NO stretch
1655[b]	Asymm C–O stretch (+NH_2 scissor)

[a] In cm^{-1}.
[b] Experimental IRMPD frequencies of ^{15}N-labelled $[Cys^{15}NO-H]^-$.

4. Conclusions

The present study has focused on the structural and vibrational features of the positive and negative ion of S-nitrosocysteine. $[SNOCys+H]^+$ and $[SNOCys-H]^-$ ions, formed by either addition or removal of a proton using ESI mass spectrometry, were found amenable to IRMPD spectroscopic assay, carried out in parallel on the ions of native cysteine. As usual, the interpretation of the IRMPD spectra has been aided by a computational survey of the IR spectra pertaining to the candidate structures for the sampled species, using hybrid DFT at the B3LYP/6-311++G** level [10,59]. At room temperature both $[SNOCys+H]^+$ and $[SNOCys-H]^-$ ions comprise a population of several conformers. The relative abundances were evaluated assuming a Maxwell-Boltzmann distribution at 298 K and were taken into account to derive a convoluted IR spectrum. The so-obtained calculated IR spectra are in good agreement with the experimental IRMPD spectra for both $[SNOCys+H]^+$ and $[SNOCys-H]^-$ ions and their ^{15}N isotopologues. This finding supports the recognition of the significant conformers contributing to the sampled ion population and allows the direct assignment of the active vibrational modes in the IRMPD spectra.

The IR features detected in the 1000–1800 cm^{-1} range (so-called IR fingerprint region) have proven to be highly informative. As already reported [29], $[Cys-H]^-$ ions do not display any

significant IRMPD activity in a relatively wide region between 1313 and 1647 cm^{-1}, namely the frequency positions of the symmetric and asymmetric $-CO_2^-$ stretching modes. It is in this blank interval that $[SNOCys-H]^-$ ions display a remarkable, ^{15}N-isotope-sensitive band. The band is assigned to the NO stretching vibration and stands out as a notable signature for S-nitrosation. A similar, clearcut piece of information cannot be gained from IRMPD spectroscopy of the positively charged $[SNOCys+H]^+$ ion. For this species the informative NO stretching mode is active at a frequency close to the C=O stretching resonance, yielding a broad, unresolved absorption. Indeed, a (partial) separation of the two modes is revealed only in the spectrum of the ^{15}N-labelled $[S^{15}NOCys+H]^+$ ion, which allowed to identify the distinct presence and activity of the two modes.

The unambiguous identification of the nitrosation feature in the IRMPD spectrum of deprotonated S-nitrosocysteine provides a characteristic signature of this modification. In a similar way, characteristic IRMPD signatures have been identified for the phosphorylation of amino acids and peptides [60–62], for the nitration of tyrosine [38] and for the sulfide to sulfoxide oxidation in methionine and related compounds [63].

Acknowledgements

Financial support was provided by the Italian Ministero dell'Istruzione, dell'Università e della Ricerca and by the European Community's Seventh Framework Programme (FP7/2007-2013, under grant agreement no. 226716) which provided also travel funding to F.L., M.E.C. and B.C. for access to the European multi-user facility CLIO. The skilful assistance of the CLIO team under the direction of J.M. Ortega and of Joel Lemaire, in charge of the beamline, is gratefully acknowledged.

Appendix A. Supplementary data

Supplementary data associated with this article can be found, in the online version, at http://dx.doi.org/10.1016/j.ijms.2012.07.003.

References

[1] D.L.H. Williams, Accounts of Chemical Research 32 (1999) 869–876.
[2] D. Giustarini, A. Milzani, R. Colombo, I. Dalle-Donne, R. Rossi, Clinica Chimica Acta 330 (2003) 85–98.
[3] M.W. Foster, T.J. McMahon, J.S. Stamler, Trends in Molecular Medicine 9 (2003) 160–168.
[4] N. Hogg, Annual Review of Pharmacology and Toxicology 42 (2002) 585–600.
[5] E. Aranda, C. Lopez-Pedrera, J.R. De La Haba-Rodriguez, A. Rodriguez-Ariza, Current Molecular Medicine 12 (2012) 50–67.
[6] L.A. Peterson, T. Wagener, H. Sies, W. Stahl, Chemical Research in Toxicology 20 (2007) 721–723.
[7] E.E. Moran, Q.K. Timerghazin, E. Kwong, A.M. English, Journal of Physical Chemistry B115 (2011) 3112–3126.
[8] M.G. de Oliveira, S.M. Shishido, A.B. Seabra, N.H. Morgon, Journal of Physical Chemistry A106 (2002) 8963–8970.
[9] L. Grossi, P.C. Montevecchi, S. Strazzari, Journal of the American Chemical Society 123 (2001) 4853–4854.
[10] J.R. Eyler, Mass Spectrometry Reviews 28 (2009) 448–467.
[11] N.C. Polfer, J. Oomens, Mass Spectrometry Reviews 28 (2009) 468–494.
[12] T.D. Fridgen, Mass Spectrometry Reviews 28 (2009) 586–607.
[13] R. Wu, T.B. McMahon, ChemPhysChem 9 (2008) 2826–2835.
[14] R. Wu, T.B. McMahon, Journal of the American Chemical Society 130 (2008) 3065–3078.
[15] R.T. Wu, B. McMahon, Angewandte Chemie International Edition 46 (2007) 3668–3671.
[16] C. Kapota, J. Lemaire, P. Maitre, G. Ohanessian, Journal of the American Chemical Society 126 (2004) 1836–1842.
[17] R.C. Dunbar, A.C. Hopkinson, J. Oomens, C.-K. Siu, K.W.M. Siu, J.D. Steill, U.H. Verkerk, J. Zhao, Journal of Physical Chemistry B113 (2009) 10403–10408.
[18] J.T. O'Brien, J.S. Prell, J.D. Steill, J. Oomens, E.R. Williams, Journal of Physical Chemistry A112 (2008) 10823–10830.
[19] M.F. Bush, J. Oomens, R.J. Saykally, E.R. Williams, Journal of the American Chemical Society 130 (2008) 6463–6471.
[20] P.B. Armentrout, M.T. Rodgers, J. Oomens, J.D. Steill, Journal of Physical Chemistry A112 (2008) 2248–2257.
[21] M.T. Rodgers, P.B. Armentrout, J. Oomens, J.D. Steill, Journal of Physical Chemistry A112 (2008) 2258–2267.
[22] M.W. Forbes, M.F. Bush, N.C. Polfer, J. Oomens, R.C. Dunbar, E.R. Williams, R.A. Jockusch, Journal of Physical Chemistry A111 (2007) 11759–11770.
[23] N.C. Polfer, J. Oomens, R.C. Dunbar, Physical Chemistry Chemical Physics 8 (2006) 2744–2751.
[24] R.C. Dunbar, N. Polfer, J. Oomens, Journal of the American Chemical Society 129 (2007) 14562–14563.
[25] N.C. Polfer, J. Oomens, D.T. Moore, G. Von Helden, G. Meijer, R.C. Dunbar, Journal of the American Chemical Society 128 (2006) 517–525.
[26] D.R. Carl, T.E. Cooper, J. Oomens, J.D. Steill, P.B. Armentrout, Physical Chemistry Chemical Physics 12 (2010) 3384–3398.
[27] M.K. Drayss, P.B. Armentrout, J. Oomens, M. Schaefer, International Journal of Mass Spectrometry 297 (2010) 18–27.
[28] M. Citir, E.M.S. Stennett, J. Oomens, J.D. Steill, M.T. Rodgers, P.B. Armentrout, International Journal of Mass Spectrometry 297 (2010) 9–17.
[29] J. Oomens, J.D. Steill, B. Redlich, Journal of the American Chemical Society 131 (2009) 4310–4319.
[30] Z. Tian, A. Pawlow, J.C. Poutsma, S.R. Kass, Journal of the American Chemical Society 129 (2007) 5403–5407.
[31] Z. Tian, S.R. Kass, Angewandte Chemie International Edition 48 (2009) 1321–1323.
[32] J.D. Steill, J. Oomens, Journal of the American Chemical Society 131 (2009) 13570–13571.
[33] J. Schmidt, M.M. Meyer, I. Spector, S.R. Kass, Journal of Physical Chemistry A115 (2011) 7625–7632.
[34] H.K. Woo, K.C. Lau, X.B. Wang, L.S. Wang, Journal of Physical Chemistry A110 (2006) 12603–12606.
[35] V. Riffet, G. Frison, G. Bouchoux, Physical Chemistry Chemical Physics 13 (2011) 18561–18580.
[36] J.S. Prell, J.T. O'Brien, E.R. Williams, Journal of the American Society for Mass Spectrometry 21 (2010) 800–809.
[37] J. Lemaire, P. Boissel, M. Heninger, G. Mauclaire, G. Bellec, H. Mestdagh, A. Simon, S. Le Caer, J.M. Ortega, F. Glotin, P. Maitre, Physical Review Letters 89 (2002) 273002–273004.
[38] R.K. Sinha, B. Chiavarino, M.E. Crestoni, D. Scuderi, S. Fornarini, International Journal of Mass Spectrometry 308 (2011) 209–216.
[39] V. Ryzhov, A.K.Y. Lam, R.A.J. O'Hair, Journal of the American Society for Mass Spectrometry 20 (2009) 985–995.
[40] R.K. Sinha, P. Maitre, S. Piccirillo, B. Chiavarino, M.E. Crestoni, S. Fornarini, Physical Chemistry Chemical Physics 12 (2010) 9794–9800.
[41] G. Rauhut, A.A. Jarzecki, P. Pulay, Journal of Computational Chemistry 18 (1997) 489–500.
[42] B. Chiavarino, M.E. Crestoni, S. Fornarini, J. Lemaire, P. Maitre, L. MacAleese, Journal of the American Chemical Society 128 (2006) 12553–12561.
[43] A.V. Soldatova, M. Ibrahim, J.S. Olson, R.S. Czernuszewicz, T.G. Spiro, Journal of the American Chemical Society 132 (2010) 4614–4625.
[44] S. Osburn, J.D. Steill, J. Oomens, R.A.J. O'Hair, M. vanIStipdonk, V. Ryzhov, Chemistry: A European Journal 17 (2011) 873–879.
[45] R.A.J. O'Hair, M.L. Styles, G.E. Reid, Journal of the American Society for Mass Spectrometry 9 (1998) 1275–1284.
[46] M. Eckersley, J.H. Bowie, R.N. Hayes, International Journal of Mass Spectrometry and Ion Processes 93 (1989) 199–213.
[47] C. Coletti, N. Re, D. Scuderi, P. Maitre, B. Chiavarino, S. Fornarini, F. Lanucara, R.K. Sinha, M.E. Crestoni, Physical Chemistry Chemical Physics 12 (2010) 13455–13467.
[48] J.A. Stearns, S. Mercier, C. Seaiby, M. Guidi, O.V. Boyarkin, T.R. Rizzo, Journal of the American Chemical Society 129 (2007) 11814–11820.
[49] P. Maitre, J. Lemaire, D. Scuderi, Physica Scripta 78 (2008) 058111/1–058111/58111.
[50] P. Milko, J. Roithova, D. Schroeder, J. Lemaire, H. Schwarz, M.C. Holthausen, Chemistry: A European Journal 14 (2008) 4318–4327.
[51] K.K. Irikura, R.D. Johnson III, R.N. Kacker, Journal of Physical Chemistry A109 (2005) 8430–8437.
[52] J.P. Merrick, D. Moran, L. Radom, Journal of Physical Chemistry 111 (2007) 11683–11700.
[53] F. Lanucara, B. Chiavarino, M.E. Crestoni, D. Scuderi, R.K. Sinha, P. Maitre, S. Fornarini, Inorganic Chemistry 50 (2011) 4445–4452.
[54] B. Chiavarino, M.E. Crestoni, S. Fornarini, F. Lanucara, J. Lemaire, P. Maitre, D. Scuderi, ChemPhysChem 9 (2008) 826–828.
[55] Q.K. Timerghazin, G.H. Peslherbe, A.M. English, Physical Chemistry Chemical Physics 10 (2008) 1532–1539.
[56] M.D. Bartberger, K.N. Houk, S.C. Powell, J.D. Mannion, K.Y. Lo, J.S. Stamler, E.J. Toone, Journal of the American Chemical Society 122 (2000) 5889–5890.
[57] N. Arulsamy, D.S. Bohle, J.A. Butt, G.J. Irvine, P.A. Jordan, E. Sagan, Journal of the American Chemical Society 121 (1999) 7115–7123.
[58] J. Yi, M.A. Khan, J. Lee, G.B. Richter-Addo, Nitric Oxide 12 (2005) 261–266.
[59] L. MacAleese, P. Maitre, Mass Spectrometry Reviews 26 (2007) 583–605.
[60] D. Scuderi, C.F. Correia, P.O. Balaj, G. Ohanessian, J. Lemaire, P. Maitre, ChemPhysChem 10 (2009) 1630–1641.
[61] C.F. Correia, P.O. Balaj, D. Scuderi, P. Maitre, G. Ohanessian, Journal of the American Chemical Society 130 (2008) 3359–3370.
[62] C.F. Correia, C. Clavaguera, U. Erlekam, D. Scuderi, G. Ohanessian, ChemPhysChem 9 (2008) 2564–2573.
[63] M. Ignasiak, D. Scuderi, P. de Oliveira, T. Pedzinski, Y. Rayah, C. Houee Levin, Chemical Physics Letters 502 (2011) 29–36.